Int. J. Heat Mass Transfer. Vol. 35, No. 12, pp. 3265–3273, 1992
Printed in Great Britain

0017-9310/92 $5.00+0.00

Thermophoresis of a radiating aerosol in thermally developing Poiseuille flow

G. JIA,† Y. YENER and J. W. CIPOLLA, JR.
Mechanical Engineering Department, Northeastern University, Boston, MA 02115, U.S.A.

(*Received* 4 *April* 1991 *and in final form* 17 *February* 1992)

Abstract—Radiation and thermophoresis interaction in thermally developing laminar flow in a constant-wall-temperature parallel-plate channel is investigated. The fluid is a radiatively nonparticipating gas containing emitting, absorbing, and isotropically scattering gray aerosol particles. The channel walls are opaque, gray and diffuse. Formal relations developed for the radiation part are used together with the discretized forms of the energy and particle conservation equations to solve the problem numerically through an iterative scheme. Various results are presented to illustrate the effects of the parameters of the problem on the temperature and particle concentration distributions, as well as on particle deposition on the channel walls when they are cold and on the development of the particle-free zone along the walls when they are hot.

INTRODUCTION

ULTRAFINE aerosols (i.e. submicrometer sized particles) suspended in a nonisothermal gas acquire a mean velocity relative to the gas and move in a direction opposite to the temperature gradient. This noncontinuum effect, known as thermophoresis, occurs whenever the size of the particles is comparable to the mean-free-path of the background gas and is caused by the differential momentum transfer to the particles following collisions with molecules that originate in regions of the gas that differ in temperature. Thermophoresis is particularly interesting when the particles are at sufficiently high temperatures to participate in radiative transfer and, therefore, are partially responsible for the temperature gradients in the gas. This case not only has intrinsic interest from a theoretical viewpoint, but is also important in a variety of engineering fields including material processing techniques that involve particle deposition from high temperature gas streams (e.g. the Modified Chemical Vapor Deposition, MCVD, process [1]), formation and motion of soot in flames and, more importantly, deposition of soot on cooled gas turbine blades [2], fouling of heat exchanger surfaces, etc. There has been very little research to date on the general problem of radiation coupled with aerosol motion through thermophoresis. However, it has already been demonstrated that thermophoresis can have a significant effect on the spatial distribution of aerosol particles and the temperature in the medium [3–6].

Simpkins *et al.* [1], Walker *et al.* [7], Weinberg and Subramanian [8] and Weinberg [9] are among the first investigators who modeled particle deposition by thermophoresis in laminar tube flow in the context of optical fiber preform fabrication by the MCVD process. Recently, the effect of laser radiation on the aerosol deposition has been studied by Morse *et al.* [10], Ravikumar [11], and Cipolla and Morse [3] and shown to be an effective mechanism to enhance aerosol deposition efficiency in the MCVD process. In these studies it has also been demonstrated that in the presence of laser radiation the aerosol can reach rather high temperatures, so that emission of thermal radiation from the aerosol should be considered in the calculation of the temperature field. More recently, Paz [12] and Paz *et al.* [13] have studied the effects of spontaneous emission from the aerosol particles generated in the MCVD process on the temperature and concentration fields, as well as on the deposition efficiency in the two limits where the aerosol can be modeled both as an optically thin medium (when the inlet concentration is below 10^{12} cm^{-3}) and an optically thick medium (for higher inlet concentrations). They have demonstrated that the inclusion of spontaneous emission from the aerosol particles reduces, in general, the temperature gradients in the flow field, thereby lowering the thermophoretic effect responsible for the aerosol deposition on the inner wall of the tube. As a consequence, they have concluded that the aerosol deposition efficiency is lower than what would be predicted if spontaneous emission were neglected.

The objective of the present work is to investigate the interaction between radiation and thermophoresis in thermally developing laminar flow in a parallel-plate channel. The aerosol particles are assumed to be absorbing, emitting, isotropically scattering and gray, with their absorption and scattering coefficients being proportional to the local concentration of particles. It is also assumed that the aerosol is dilute, mono-

† Present address: Senior Engineer, Thermoflow Inc., 888 Worcester Street, Wellesley, MA 02181, U.S.A.

NOMENCLATURE

C	aerosol particle concentration
c_p	specific heat of background gas
D	Brownian diffusion coefficient
D_e	equivalent diameter, $4L$
E	particle deposition efficiency, equation (19)
E_n	exponential integral function
G	dimensionless incident radiation
J_w	local flux of particles to cold channel walls
$\bar{J}_w$	dimensionless local particle wall flux, $J_w/4C_iU_m/Pe$
K	thermophoretic coefficient
k	thermal conductivity of background gas
L	half the distance between channel walls
N_{CR}	conduction-to-radiation parameter, equation (4)
Nu	local Nusselt number
n	refractive index of gas–aerosol mixture
Pe	Peclet number, $Re\ Pr$
Pr	Prandtl number, $\rho\nu c_p/k$
Q^r	dimensionless radiative heat flux, $q^r/4n^2\bar{\sigma}T_w^4$
Q^T	dimensionless total heat flux
q^r	radiative heat flux in y-direction
Re	Reynolds number, U_mD_e/ν
Sc	Schmidt number, ν/D
T	temperature
U_m	mean flow velocity
u	fully-developed velocity profile, $\frac{3}{2}U_m(1-\eta^2)$
x	axial coordinate
y	transverse coordinate.

Greek symbols

ε	emissivity
η	dimensionless transverse coordinate, y/L
Θ	dimensionless temperature, T/T_w
Θ_b	dimensionless bulk temperature, equation (15)
κ	absorption coefficient
μ	direction cosine
ν	kinematic viscosity of background gas
ξ	dimensionless axial coordinate, $(32/3)(x/D_e)/(Re\ Pr)$
ρ	density of background gas
σ	scattering coefficient
$\bar{\sigma}$	Stefan–Boltzmann constant
τ	local optical variable
τ_0	local optical thickness
τ_0^*	optical thickness at $x=0$, $\tau_0(0)$
ϕ	dimensionless concentration, C/C_i
Ψ	dimensionless radiation intensity
ω	scattering albedo.

Superscripts

+	forward flux
−	backward flux.

Subscripts

i	quantities evaluated at channel entrance
nr	no-radiation quantity
w	quantities evaluated at channel walls
0	quantities evaluated at $x=0$.

disperse, nonreactive and in thermal equilibrium with the radiatively nonparticipating carrier gas. In the following sections we first present the formulation of the problem with the assumption of constant thermophysical and transport properties. Next, we develop a formal solution to the radiation part of the problem, and use it together with the discretized forms of the energy and particle conservation equations to solve the problem numerically through an iterative scheme. Finally, we present results illustrating the effects of various parameters of the problem on the temperature and particle concentration distributions, as well as on the particle deposition efficiency along the channel when the channel walls are cold and on the development of the particle-free zone along walls when they are hot.

FORMULATION

Consider the thermally developing steady laminar flow of a gas containing suspended aerosol particles between two infinite parallel plates separated by a distance $2L$. The aerosol particles are assumed to be absorbing, emitting, isotropically scattering and gray. The bounding surfaces, located at $y=\mp L$, are considered to be impermeable, opaque, gray, diffuse reflectors and diffuse emitters, with the same uniform emissivity over each surface. The gas enters the cooled (or heated) section of the channel at the origin of the axial coordinate x with a fully-developed velocity profile $u(y)$, uniform temperature T_i and aerosol particle concentration C_i, while the channel walls are maintained isothermal at T_w for $x \geqslant 0$. It is also assumed that the aerosol is monodisperse, dilute, nonreactive and in thermal equilibrium with the radiatively nonparticipating background gas. Moreover, the aerosol particles are small enough for inertial effects to be ignored. Aerosol particles may be assumed to be in thermal equilibrium with the background gas if the thermal response time of the particles is small compared to the characteristic time of the changing flow conditions. For 1.0 μm diameter SiO_2 particles, for example, the thermal response time is about 2.5 μs, so thermal equilibrium of such particles

within a fully-developed laminar flow channel seems reasonable. Also, ultrafine aerosol particles rapidly achieve hydrodynamic equilibrium. For example, a 10 μm diameter aerosol particle of unit density placed at rest in a gas flow of 10 m s^{-1} will reach hydrodynamic equilibrium with the flow after travelling 3.6×10^{-5} m [14].

Assuming constant thermophysical and transport properties for the aerosol–gas mixture, and neglecting viscous dissipation as well as axial heat conduction, radiation, Brownian diffusion and thermophoretic motion of the aerosol particles, the energy and the particle conservation equations may be written in dimensionless form as

$$(1-\eta^2)\frac{\partial\Theta}{\partial\xi}=\frac{\partial^2\Theta}{\partial\eta^2}-\frac{\tau_0^*}{N_{CR}}\frac{\partial Q^r}{\partial\eta} \tag{1}$$

and

$$(1-\eta^2)\frac{\partial\phi}{\partial\xi}=\frac{Pr}{Sc}\frac{\partial^2\phi}{\partial\eta^2}+K\,Pr\frac{\partial}{\partial\eta}\left(\frac{\phi}{\Theta}\frac{\partial\Theta}{\partial\eta}\right), \tag{2}$$

with the inlet and boundary conditions

$$\Theta(0,\eta)=\Theta_i,\quad \phi(0,\eta)=1 \tag{3a,b}$$

$$\frac{\partial\Theta(\xi,0)}{\partial\eta}=0,\quad \frac{\partial\phi(\xi,0)}{\partial\eta}=0 \tag{3c,d}$$

$$\Theta(\xi,1)=1,\quad \phi(\xi,1)=0. \tag{3e,f}$$

In equation (1), $\tau_0^*=(\kappa_0+\sigma_0)L$, and the conduction-to-radiation parameter N_{CR} is given by

$$N_{CR}=\frac{k(\kappa_0+\sigma_0)}{4n^2\bar{\sigma}T_w^3} \tag{4}$$

where κ_0 and σ_0 are, respectively, the absorption and scattering coefficients of the mixture at the entrance of the channel. Also, n denotes the refractive index of the mixture, which is assumed to be constant, and $\bar{\sigma}$ is the Stefan–Boltzmann constant. Furthermore, in equation (2), $Sc=\nu/D$ represents the Schmidt number, where D denotes the Brownian diffusion coefficient and K is the thermophoretic coefficient. Both D and K are considered to be independent of temperature in this work. In equation (1), the dimensionless radiative heat flux Q^r is defined as

$$Q^r(\xi,\eta)=Q^+(\xi,\eta)-Q^-(\xi,\eta) \tag{5}$$

with

$$Q^{\pm}(\xi,\eta)=\frac{1}{2}\int_0^1\Psi(\xi,\eta,\pm\mu)\mu\,d\mu \tag{6}$$

where $\Psi(\xi,\eta,\mu)$ represents the dimensionless radiation intensity and μ is the direction cosine (as measured from the positive y-axis) of the propagating radiation in the gas–aerosol mixture. On the other hand, if the absorption and the scattering coefficients are both considered to be proportional to the aerosol concentration $\phi(\xi,\eta)$ according to

$$\kappa(\xi,\eta)=\kappa_0\phi(\xi,\eta)\quad\text{and}\quad\sigma(\xi,\eta)=\sigma_0\phi(\xi,\eta) \tag{7a,b}$$

then, with the assumption that the mixture is locally plane-parallel, the dimensionless radiation intensity satisfies the radiative transfer equation given in the form

$$\mu\frac{\partial\Psi}{\partial\tau}+\Psi(\xi,\tau,\mu)=(1-\omega)\Theta^4(\xi,\tau)+\frac{\omega}{2}\int_{-1}^1\Psi(\xi,\tau,\mu')\,d\mu' \tag{8}$$

where

$$0<\tau(\xi,\eta)<\tau_0(\xi),\quad -1\leqslant\mu\leqslant1.$$

In equation (8), axial variations of Ψ have been neglected compared to variations normal to the flow and $\omega=\sigma_0/(\kappa_0+\sigma_0)$ represents the scattering albedo. Furthermore, the quantity τ denotes the local optical variable defined as

$$\tau(\xi,\eta)=\tau_0^*\int_0^\eta\phi(\xi,\eta')\,d\eta' \tag{9}$$

and $\tau_0(\xi)=\tau(\xi,1)$ represents the local optical thickness at the dimensionless axial location ξ, with $\tau_0^*\equiv\tau_0(0)$ being the optical thickness at $\xi=0$.

Assuming that both plates have the same radiative properties, the boundary conditions for equation (8) are given by

$$\Psi(\xi,0,\mu)=\Psi(\xi,0,-\mu),\quad \mu>0 \tag{10a}$$

$$\Psi(\xi,\tau_0,-\mu)=\varepsilon_w+2(1-\varepsilon_w)\times\int_0^1\Psi(\xi,\tau_0,\mu')\mu'\,d\mu',\quad \mu>0. \tag{10b}$$

It can be shown that the derivative of the radiative heat flux in the energy equation (1) is given by

$$\frac{\partial Q^r}{\partial\eta}=(1-\omega)\tau_0^*\phi(\xi,\tau)[\Theta^4(\xi,\tau)-G(\xi,\tau)] \tag{11}$$

where

$$G(\xi,\tau)=\frac{1}{2}\int_{-1}^1\Psi(\xi,\tau,\mu)\,d\mu \tag{12}$$

represents the dimensionless incident radiation.

It is obvious from equation (2) that the temperature distribution $\Theta(\xi,\eta)$ has to be known in order to obtain the aerosol concentration distribution $\phi(\xi,\eta)$ in the flow field. On the other hand, the energy equation (1) contains a source term which depends on the derivative of the radiative heat flux. The radiative heat flux, which is to be determined from the solution of the radiative transfer equation (8) with the boundary conditions (10), in turn, depends on the aerosol concentration distribution as indicated by equations (9) and (11). Thus, the energy, particle concentration and radiative transfer equations are nonlinearly coupled to each other, and an iterative scheme is needed to solve them simultaneously.

Local Nusselt number

Once the temperature distribution in the flow is determined, the local Nusselt number is obtained from its definition as

$$Nu(\xi) = \frac{4Q_w^T(\xi)}{\Theta_b(\xi) - 1} \tag{13}$$

where the dimensionless total wall heat flux Q_w^T is obtained from

$$Q_w^T(\xi) = -\frac{\partial\Theta(\xi, 1)}{\partial\eta} + \frac{\tau_0^*}{N_{CR}} Q^r(\xi, 1) \tag{14}$$

and Θ_b represents the dimensionless bulk temperature defined as

$$\Theta_b(\xi) = \frac{3}{2}\int_0^1 \Theta(\xi, \eta)(1-\eta^2)\, d\eta. \tag{15}$$

In equation (14), the first term on the right-hand side is the dimensionless heat flux due to conduction and the second term is the dimensionless radiation heat flux, both at the channel walls.

Particle deposition at the channel walls

Generally speaking, if $\Theta(\xi, \eta)$ is known, then equation (2) can readily be solved to obtain the particle concentration distribution $\phi(\xi, \eta)$. On the other hand, for aerosol particles of interest (in air at normal temperature and pressure) the Schmidt number is very large, of the order of magnitude of 10^3 to 10^5. For example, for a spherical particle of 1 μm diameter in air, the Schmidt number is of order 10^5. Accordingly, in equation (2), the Brownian diffusion may be neglected compared to convection and thermophoretic motion of the particles, and therefore the particle conservation equation reduces to

$$(1-\eta^2)\frac{\partial\phi}{\partial\xi} = K\,Pr\frac{\partial}{\eta}\left(\frac{\phi}{\Theta}\frac{\partial\Theta}{\partial\eta}\right) \tag{16}$$

with the inlet and boundary conditions

$$\phi(0, \eta) = 1 \quad \text{and} \quad \frac{\partial\phi(\xi, 0)}{\partial\eta} = 0. \tag{17a,b}$$

In this limit the contribution of Brownian diffusion is much smaller than that of thermophoresis except within the extremely thin Brownian diffusion sublayer on the channel walls, where the temperature gradients are very small and thermophoresis virtually plays no role at all. In the absence of Brownian diffusion, equation (16) is of first order in η, thus requiring only one boundary condition in the η-direction as stated by equation (17b), and the boundary condition (3f) is no longer imposed. The solution of equation (16) then yields a non-zero particle concentration at the boundaries when the plates are colder than the incoming flow. Strictly speaking, the nonzero concentration is the one at the outer edge of the very thin Brownian sublayer where the gas velocity is so small that particles entering this layer by thermophoresis deposit on the walls at the same axial location due to London-van der Waals forces. Thus, the local flux of particles J_w to the (cold) channel walls will be given by the thermophoretic flux to the thin sublayer and can be calculated, in dimensionless form, from

$$\bar{J}_w = -K\,Pr\left(\frac{\phi}{\Theta}\frac{\partial\Theta}{\partial\eta}\right)_{\eta=1}. \tag{18}$$

The particle deposition efficiency $E(\xi)$ is defined as the fraction of aerosol particles entering the channel at $\xi = 0$ that have deposited on the walls from $\xi = 0$ to ξ. Since the total number of particles entering the channel at $\xi = 0$ must be equal to the number of particles deposited on the walls plus the total number of particles crossing the channel with flow at ξ, one can show that

$$E(\xi) = 1 - \frac{2}{3}\int_0^1 (1-\eta^2)\phi(\xi, \eta)\, d\eta. \tag{19}$$

In this section we have presented a formulation of the problem. In the following section, we give a method for the determination of the radiative heat flux Q^r and its derivative $\partial Q^r/\partial\tau$ in terms of the temperature distribution in the flow.

FORMAL SOLUTION TO THE RADIATION PART

The solution of the problem defined by the radiative transfer equation (8) and the boundary conditions (10a,b) can be written as

$$\Psi(\xi, \tau, \mu) = \Psi_1(\xi, \tau, \mu) + J(\xi)[1 + \Psi_2(\tau, \mu)] \tag{20}$$

where

$$J(\xi) = \varepsilon_w + 4(1-\varepsilon_w)Q^+(\xi, \tau_0) \tag{21}$$

and Ψ_i are the solutions of the following two auxiliary problems:

$$\mu\frac{\partial\Psi_i}{\partial\tau} + \Psi_i(\xi, \tau, \mu) = S_i(\xi, \tau), \quad i = 1, 2 \tag{22}$$

$$\Psi_i(\xi, 0, \mu) = \Psi_i(\xi, 0, -\mu), \quad \mu > 0 \tag{23a}$$

$$\Psi_i(\xi, \tau_0, -\mu) = 0, \quad \mu > 0. \tag{23b}$$

In equation (22), the source functions S_i are given by

$$S_i(\xi, \tau) = (1-\omega)[\delta_{i1}\Theta^4(\xi, \tau) + \delta_{i2}] + \omega G_i(\xi, \tau) \tag{24}$$

where δ_{ij} denotes the Kronecker delta and $G_i(\xi, \tau)$ are defined in terms of Ψ_i according to equation (12).

Substituting the superposition (20) into equations (5) and (6) gives

$$Q^r(\xi, \tau) = Q_1^r(\xi, \tau) + J(\xi)Q_2^r(\tau) \tag{25}$$

with

$$Q_i^r(\xi, \tau) = Q_i^+(\xi, \tau) - Q_i^-(\xi, \tau) \tag{26}$$

where $Q_i^\pm$ are defined in terms of Ψ_i according to

equation (6). Also, substituting equation (20) into equation (21) gives

$$J_w(\xi) = \frac{\varepsilon_w + 4(1-\varepsilon_w)Q_1^+(\xi,\tau_0)}{\varepsilon_w - 4(1-\varepsilon_w)Q_2^+(\tau_0)}. \quad (27)$$

It can be shown by first solving the problem defined by equations (22) and (23) for Ψ_i in terms of S_i and then substituting Ψ_i into equation (6) that

$$Q_i^+(\xi,\tau) = \frac{1}{2}\left\{\int_0^\tau S_i(\xi,\tau')E_2(\tau-\tau')\,d\tau' + \int_0^{\tau_0} S_i(\xi,\tau')E_2(\tau+\tau')\,d\tau'\right\} \quad (28a)$$

and

$$Q_i^-(\xi,\tau) = \frac{1}{2}\left\{\int_\tau^{\tau_0} S_i(\xi,\tau')E_2(\tau'-\tau)\,d\tau'\right\}. \quad (28b)$$

Substituting the superposition (21) into equation (12) also gives

$$G(\xi,\tau) = G_1(\xi,\tau) + J(\xi)\{1+G_2(\tau)\} \quad (29)$$

and it can be shown that

$$G_i(\xi,\tau) = \frac{1}{2}\int_0^{\tau_0} [E_1(\tau+\tau') + E_1(|\tau-\tau'|)]S_i(\xi,\tau')\,d\tau'. \quad (30)$$

In equations (28) and (30), $E_n(x)$ represents the exponential integral function.

By combining equations (24) and (30), it can further be shown that the source functions S_i satisfy the following singular Fredholm integral equation:

$$S_i(\xi,\tau) = F_i(\xi,\tau) + \frac{\omega}{2}\int_0^{\tau_0} K(\tau,\tau')S_i(\xi,\tau')\,d\tau' \quad (31)$$

where

$$F_i(\xi,\tau) = (1-\omega)[\delta_{i1}\Theta^4(\xi,\tau) - \delta_{i2}] \quad (32)$$

and the kernel $K(\tau,\tau')$ is given by

$$K(\tau,\tau') = E_1(\tau+\tau') + E_1(|\tau-\tau'|). \quad (33)$$

Following the work of Özışık and Yener [15], we now expand S_i into a power series as

$$S_i(\xi,\tau) = \sum_{n=0}^{N} C_{in}(\xi)\tau^n \quad (34)$$

and then substitute it into the integral equation (31). Next, we multiply the resulting equation by τ^m and then integrate it over τ from 0 to τ_0 to obtain the following system of $N+1$ algebraic equations for the expansion coefficients C_{in}:

$$\sum_{n=0}^{N} B_{mn}C_{in}(\xi) = A_{im}(\xi), \quad m = 0, 1, \ldots, N \quad (35)$$

where

$$A_{im}(\xi) = (1-\omega)\left\{\delta_{i1}\int_0^{\tau_0}\Theta^4(\xi,\tau)\tau^m\,d\tau - \delta_{i2}\frac{\tau_0^{m+1}}{m+1}\right\} \quad (36)$$

and

$$B_{mn} = \frac{\tau_0^{m+n+1}}{m+n+1} - \frac{\omega}{2}\int_0^{\tau_0}\int_0^{\tau_0}\tau'^n\tau^m K(\tau,\tau')\,d\tau'\,d\tau. \quad (37)$$

Once the expansion coefficients $C_{in}(\xi)$ are obtained from the solution of equation (35), the forward and backward radiative fluxes and the incident radiation functions can readily be determined by substituting the expansion (34) for S_i into equations (28a,b) and (30) as

$$Q_i^+(\xi,\tau) = \frac{1}{2}\sum_{n=0}^{N} C_{in}(\xi)\left\{\int_0^\tau \tau'^n E_2(\tau-\tau')\,d\tau' + \int_0^{\tau_0} E_2(\tau+\tau')\tau'^n\,d\tau'\right\} \quad (38a)$$

$$Q_i^-(\xi,\tau) = \frac{1}{2}\sum_{n=0}^{N} C_{in}(\xi)\int_0^{\tau_0} E_2(\tau'-\tau)\tau'^n\,d\tau' \quad (38b)$$

and

$$G_i(\xi,\tau) = \frac{1}{2}\sum_{n=0}^{N} C_{in}(\xi)\int_0^{\tau_0}[E_1(\tau+\tau') + E_1(|\tau-\tau'|)]\tau'^n\,d\tau'. \quad (39)$$

Equations (37), (38a,b) and (39) involve integrals of the exponential integral functions. In this work we have evaluated these integrals analytically and the results can be found in ref. [16].

SOLUTION

Having established the formulation of the problem, the solution of the interaction problem is now reduced to that of iterative calculations between the formal relations for Q^r and $\partial Q^r/\partial\tau$ and a numerical solution of the energy and particle conservation equations.

Cold wall case

When the channel walls are colder than the incoming aerosol–gas mixture, particles will deposit on the walls due to thermophoresis as the flow proceeds in the channel. However, as the gas flows downstream its temperature will gradually approach the wall temperature and the thermophoretic deposition will eventually cease; therefore, not all the particles initially present in the flow will be captured. As discussed earlier, the Brownian diffusion term in the particle concentration equation (2) does not play a role in the calculation of the concentration field, except in the extremely thin diffusion layer adjacent to the channel walls. Without the diffusion term, the

solution of the particle concentration equation yields nonzero concentration at the walls. For the cold wall case, this nonzero wall concentration is used together with the thermophoretic velocity of the particles to calculate the particle flux to the walls. The numerical procedure employed in this case can be outlined as follows. The energy equation (1) is first solved at the axial location ξ_1 numerically by the Crank–Nicolson scheme in the absence of radiation to obtain the no-radiation temperature profile $\Theta_{nr}(\xi_1, \eta)$. This profile is then used in the numerical solution (again by the Crank–Nicolson scheme) of the particle conservation equation (2) to obtain the no-radiation concentration profile $\phi_{nr}(\xi_1, \eta)$. Next, the temperature profile $\Theta_{nr}(\xi_1, \eta)$ is transformed to the form $\Theta_{nr}(\xi_1, \tau)$ by the use of relation (9). The temperature profile $\Theta_{nr}(\xi_1, \tau)$ is now used as a first guess in the solution of the radiative transfer equation (8), and the relations developed in the previous section are employed to determine $Q^r(\xi_1, \tau)$, which is, in turn, transformed to the form $Q^r(\xi_1, \eta)$, again by the use of relation (9), and is used in the numerical solution of the energy equation (1) to obtain a new temperature profile $\Theta(\xi_1, \eta)$. This new temperature profile is subsequently used as the next guess to first obtain a new $\phi(\xi_1, \eta)$ and then $\Theta(\xi_1, \eta)$ by repeating the above described scheme. This procedure is repeated until the differences between the last two calculated profiles for $\Theta(\xi_1, \eta)$ and $\phi(\xi_1, \eta)$ satisfy prescribed accuracies. Once the desired accuracies are reached, the dimensionless heat and particle fluxes to the boundaries are calculated at ξ_1, respectively, from equations (14) and (18). When the calculations are completed at ξ_1, the above procedure is repeated at the following axial locations ξ_i, $i = 2, 3, \ldots$, where at each location ξ_{i+1} the temperature profile at the previous location ξ_i is taken as the first guess. For the results presented here, the subdivisions in the transverse η-direction were nonuniformly spaced, with higher concentration of grid points near the walls; the smallest grid size next to the boundaries was $\Delta\eta = 0.005$ and the total number of grid points was 200. However, various numerical experiments were carried out with grid points in the range 100–500 over $\eta \in (0, 1)$ to verify that the solutions were grid independent. In the streamwise direction, the first step size in the ξ-direction was taken to be as small as 0.0003, for cases in which the radiation was strong, with the step sizes increasing further from the inlet. Convergence was assumed to have been reached when the maximum relative difference in sequential iterates was less than 10^{-4} over all grid points for both the temperature and concentration fields.

Hot wall case

When the channel walls are hot, the particles are pushed away from the walls, giving rise to a particle-free region along the walls. Actually, the trajectory of the particles departing from the channel walls at $\xi = 0$ determines the boundary of the particle-free region. It would be relatively easy to determine this trajectory for the high-Schmidt-number flow if the energy and particle conservation equations were not coupled, because, in that case, the axial velocity of the particles would be the same as the axial velocity of the carrier gas and the transverse component would readily be calculated from the already-obtained temperature profiles. However, in the present case, the energy, radiative transfer and particle conservation equations are highly nonlinearly coupled, making the determination of the boundary of the particle-free zone a difficult task. The iterative numerical solution procedure employed in this case is essentially the same as in the previous case. We have, however, incorporated a mass conservation scheme [12] into the numerical solution of the particle conservation equation (16) by controlling two criteria: the first one is that the total number of aerosol particles crossing the channel at each axial location is the same since there is no particle deposition, and the second is that the

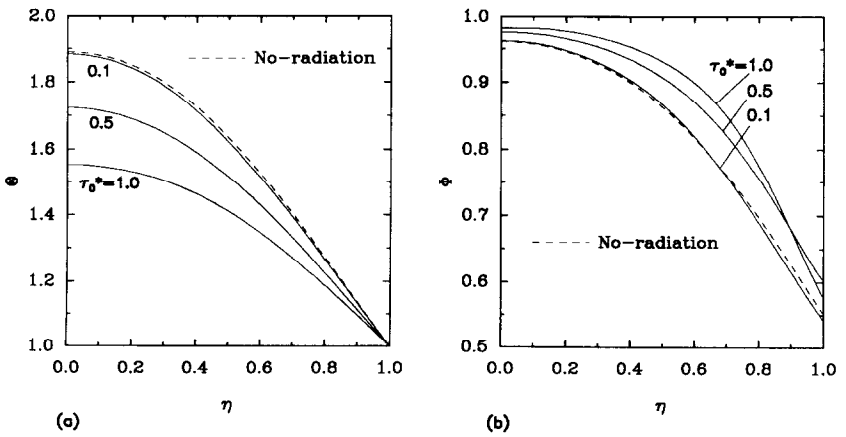

FIG. 1. Effect of the optical thickness τ_0^* at $\xi = 0.1$ on the temperature profile (a) and the concentration profile (b). $\Theta_i = 2.0$, $\omega = 0.5$, $\varepsilon_w = 1.0$, $N_{CR} = 0.5$ and $K\,Pr = 0.7$.

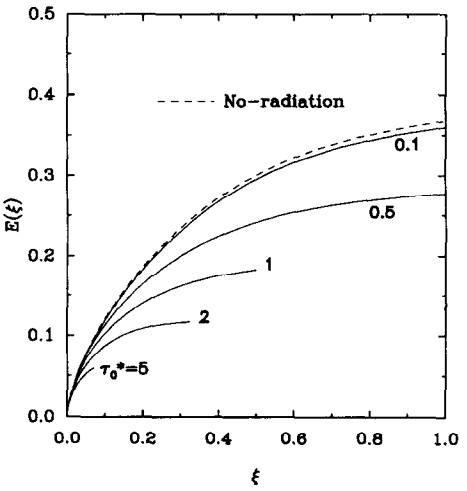

FIG. 2. Effect of the optical thickness τ_0^* on the particle deposition efficiency. $\Theta_i = 2.0$, $\omega = 0.5$, $\varepsilon_w = 1.0$, $N_{CR} = 0.5$ and $K\,Pr = 0.7$.

concentration in the particle-free zone cannot be negative. We have also used an approximation in the form $\tau(\xi, \eta) \cong \tau_0^* \eta$ instead of relation (9) for the transformations between the physical variable η and the optical variable τ at each ξ_i. This approximation was prompted by the numerical difficulties arising from the fact that over the thickness of the particle-free region the particle concentration is zero and, therefore, the optical variable does not vary, whereas there are significant variations in temperature in the same region.

RESULTS AND DISCUSSION

A selection of numerical results that demonstrate the effects of the principal parameters of the problem is presented in this section. Figure 1 illustrates the effect of the optical thickness τ_0^* on the temperature and aerosol concentration profiles at $\xi = 0.1$ along the channel for $\Theta_i = 2.0$ (cold boundaries) with $\omega = 0.5$, $\varepsilon_w = 1.0$, $N_{CR} = 0.5$ and $K\,Pr = 0.7$. With large values of τ_0^*, radiation has a stronger effect on the heat transfer and, therefore, the temperature of the aerosol–gas mixture decays faster along the channel, resulting in less particle deposition on the channel walls. As seen from these figures, the effect is less significant for the optically thin case of $\tau_0^* = 0.1$. Figure 2, on the other hand, shows the effect of τ_0^* on the particle deposition efficiency as a function of ξ along the channel. As seen from this figure, the efficiency at any axial location decreases significantly as radiation becomes more dominant with increasing values of τ_0^*. Especially in the optically thick case of $\tau_0^* = 5$, in which radiation significantly dominates the heat transfer process, the temperature of the mixture rapidly declines to the wall temperature and the particle deposition on the plates ceases after a very short distance from the entrance. Also, in each case, the efficiency rapidly approaches an asymptotic limit. This limit is referred to as the total or overall efficiency and the length of the deposition region is determined by the distance it takes for the deposition efficiency to reach its asymptotic value. Figure 3(a) illustrates the effect of τ_0^* on the dimensionless total Q_w^T and radiative Q_w^r heat fluxes at the channel walls, and Fig. 3(b) demonstrates the effect of τ_0^* on the local Nusselt number $Nu(\xi)$. As seen from Fig. 3(b), in the optically thin case (i.e. when $\tau_0^* = 0.1$), except in regions where $\xi \ll 1$, the total heat flux slightly deviates from the no-radiation heat flux $Q_{w,nr}^T$, indicating that the decrease in the conduction heat flux because of the decreased temperature gradients is merely compensated by the radiative heat flux. For the case of large τ_0^* (i.e. when $\tau_0^* = 1.0$), radiation greatly enhances the total heat flux in regions close to the inlet (i.e. when $\xi < 0.2$), whereas the total flux is reduced at larger values of the axial locations in spite of the presence of radiation because of the significantly reduced conduction. Figure 3(b) depicts

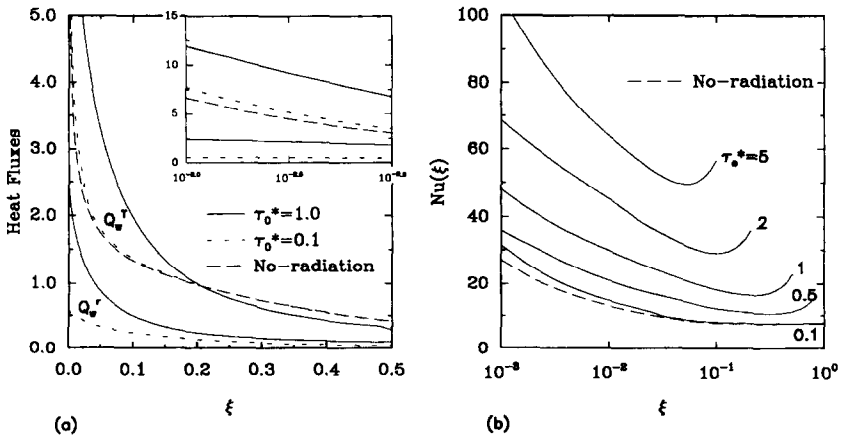

FIG. 3. Effect of the optical thickness τ_0^* on the total and radiative heat fluxes (a) and the local Nusselt number (b). $\Theta_i = 2.0$, $\omega = 0.5$, $\varepsilon_w = 1.0$, $N_{CR} = 0.5$ and $K\,Pr = 0.7$.

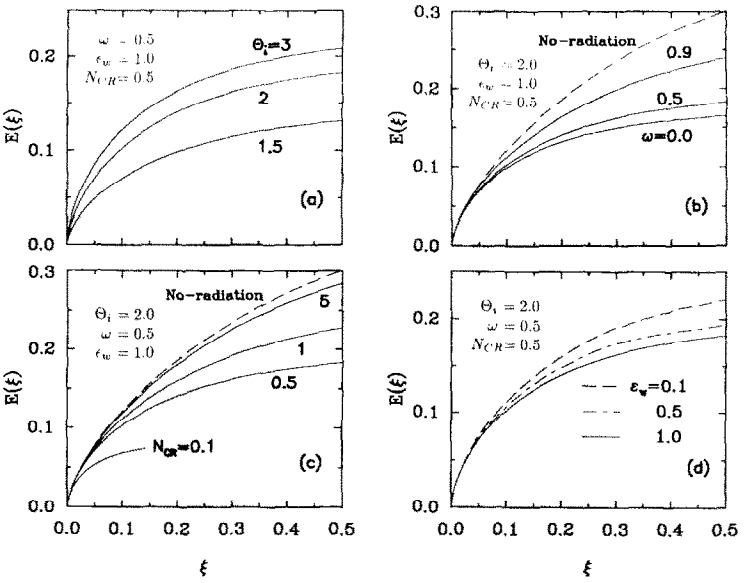

FIG. 4. The particle deposition efficiency: the effects of the inlet temperature (a), the scattering albedo (b), the conduction-to-radiation parameter (c) and the emissivity (d). $\tau_0^* = 1.0$ and $K\,Pr = 0.7$.

that the effect of τ_0^* on the local Nusselt number is significantly pronounced for larger values of τ_0^* as radiation becomes more dominant with increasing values of τ_0^*. When radiation is strong (i.e. large τ_0^*), the local Nusselt number does not seem to approach an asymptotic value. This same behavior was also observed previously by various investigators [17–20].

Figure 4(a) illustrates the effect of the inlet temperature Θ_i on the particle deposition efficiency. As expected, with larger values of Θ_i, the deposition efficiency increases. Figure 4(b), on the other hand, shows the effect of the scattering albedo ω on the deposition efficiency. The case $\omega = 0$ corresponds to purely absorbing and emitting aerosols and the effect of radiation is maximum. On the other hand, the case $\omega = 1$ corresponds to a purely scattering aerosol–gas mixture in which the radiation is uncoupled from convection and thermophoresis. Thus, as seen in Fig. 4(b), as ω approaches unity, the effects of radiation are weakened and the problem reduces to that of the nonradiating flow case. Figure 4(c) shows the effect of the conduction-to-radiation parameter N_{CR} on the deposition efficiency. It is obvious that radiation becomes the primary means of heat transfer as N_{CR} becomes smaller, and Fig. 4(c) clearly illustrates this effect on the deposition efficiency. Figure 4(d) demonstrates the effect of the boundary emissivity ε_w on the deposition efficiency. Again as expected, the black boundaries (i.e. $\varepsilon_w = 1$) cause the largest radiation effect. The results presented so far all pertain to the cold channel wall cases.

When the walls are at a higher temperature than

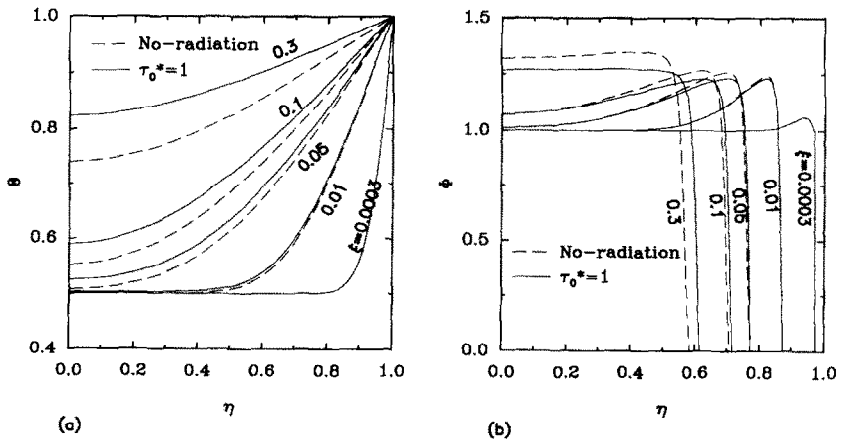

FIG. 5. Temperature and concentration profiles at various axial locations for the hot wall case. $\Theta_i = 0.5$, $\omega = 0.5$, $\varepsilon_w = 1.0$, $N_{CR} = 0.5$ and $K\,Pr = 0.7$.

the incoming aerosol–gas mixture, the aerosol particles are pushed away from the walls by thermophoresis, resulting in a particle-free region next to the walls. Figure 5(a) depicts the temperature profiles at different axial locations for the nonradiating case and the case of radiating flow with $\tau_0^* = 1.0$. Figure 5(b), on the other hand, illustrates the particle concentration profiles at the same axial locations. As seen from Fig. 5(b), the aerosol particles are pushed gradually toward the center of the channel and the thickness of the particle-free zone increases with ξ. Also, the thickness of the particle-free zone at any axial location for the nonradiating flow case is thicker than that of the radiating case. This is a result of the fact that the temperature profiles, as depicted in Fig. 5(a), are flattened in the presence of radiation, leading to reduced thermophoretic velocities away from the channel walls.

Acknowledgement—This work was partially supported by the National Science Foundation through Grant CBT-8603634.

REFERENCES

1. P. G. Simpkins, S. Greenberg-Kosinski and J. B. MacChesney, Thermophoresis: the mass transfer mechanism in modified chemical vapor deposition, *J. Appl. Phys.* **50,** 5676–5681 (1979).
2. G. Vermes, Thermophoresis-enhanced deposition rates in combustion turbine blade passages, *J. Engng Pwr* **101,** 542–548 (1979).
3. J. W. Cipolla, Jr. and T. F. Morse, Thermophoresis in an absorbing aerosol, *J. Aerosol Sci.* **18,** 245–260 (1987).
4. T. S. Tse, Y. Yener and J. W. Cipolla, Jr., Aerosol thermophoresis and radiative transfer. In *Fundamentals and Applications of Radiation Heat Transfer* (Edited by A. M. Smith and T. F. Smith), ASME/HTD Vol. 72, pp. 59–65 (1987).
5. C. Hannon, Y. Yener and J. W. Cipolla, Jr., Aerosol thermophoresis with conduction and radiation. In *Heat Transfer Phenomena in Radiation, Combustion, and Fires* (Edited by R. K. Shah), ASME/HTD Vol. 106, pp. 147–155 (1989).
6. G. Jia, J. W. Cipolla, Jr. and Y. Yener, Thermophoresis of a radiating aerosol in laminar boundary layer flow, *J. Thermophys. Heat Transfer* (accepted for publication).
7. K. L. Walker, F. T. Geyling and S. R. Nagel, Thermophoretic deposition of small particles in the modified chemical vapor deposition (MCVD) process, *J. Am. Ceram. Soc.* **63,** 552–558 (1980).
8. M. Weinberg and R. S. Subramanian, Thermophoretic deposition in a tube with variable wall temperature, *J. Colloid Interface Sci.* **87,** 579–580 (1982).
9. M. Weinberg, Thermophoretic efficiency in the modified chemical vapor deposition process, *J. Am. Ceram. Soc.* **65,** 81–87 (1982).
10. T. F. Morse, C. Y. Wang and J. W. Cipolla, Jr., Laser-induced thermophoresis and particulate deposition efficiency, *J. Heat Transfer* **107,** 155–160 (1985).
11. S. Ravikumar, Thermal radiation and thermophoresis in aerosols, Ph.D. Thesis, Northeastern University, Boston, Massachusetts (1985).
12. L. P. Paz, The effects of thermal radiation on the laser enhanced MCVD process, Ph.D. Thesis, Northeastern University, Boston, Massachusetts (1990).
13. L. P. Paz, J. W. Cipolla, Jr. and T. F. Morse, The effects of radiation on particle deposition in MCDV: the optically thin case. In *Heat Transfer Phenomena in Radiation, Combustion, and Fires* (Edited by R. K. Shah), ASME/HTD Vol. 106, pp. 157–163 (1989).
14. W. C. Hinds, *Aerosol Technology*. Wiley, New York (1982).
15. M. N. Özışık and Y. Yener, The Galerkin method for solving radiation transfer in plane-parallel participating media, *J. Heat Transfer* **104,** 351–354 (1982).
16. G. Jia, Interactions of radiation with conduction, convection and thermophoresis, Ph.D. Thesis, Northeastern University, Boston, Massachusetts (1991).
17. C. C. Lii and M. N. Özışık, Heat transfer in an absorbing, emitting and scattering slug flow between parallel plates, *J. Heat Transfer* **95,** 538–540 (1973).
18. T. C. Chawla and S. H. Chan, Spline collocation solution of combined radiation–convection in thermally developing flows with scattering, *Numer. Heat Transfer* **3,** 47–76 (1980).
19. F. H. Azad and M. F. Modest, Combined radiation and convection in absorbing, emitting and anisotropically scattering gas–particulate tube flow, *Int. J. Heat Mass Transfer* **24,** 1681–1697 (1981).
20. M. P. Mengüç, Y. Yener and M. N. Özışık, Interaction of radiation and convection in thermally developing laminar flow in a parallel-plate channel, ASME Paper 83-HT-35 (1983).